nature neuroscience

Reversed theta sequences of hippocampal cell assemblies during backward travel

Anne Cei[1,2], Gabrielle Girardeau[1,2], Céline Drieu[1,2], Karim El Kanbi[1,2] & Michaël Zugaro[1,2]

Hippocampal cell assemblies coding for past, present and future events form theta-timescale (~100 ms) sequences that represent spatio-temporal episodes. However, the underlying mechanisms remain largely unknown. We recorded hippocampal and entorhinal cortical activity as rats experienced backward travel on a model train. Although the firing fields of place cells remained stable, the order in which they were activated in the theta sequence was reversed during backward travel. Thus, hippocampal cell assemblies coordinated their relative timing to correctly predict the sequential traversal of place fields in reverse order. At the single-cell level, theta phase represented distance traveled through the field, even though the head of the rat was oriented opposite to travel direction and entorhinal head-direction cells maintained their preferred firing direction. Our results challenge most theoretical models of theta sequence generation in the hippocampus.

Hippocampal place cells selectively discharge in specific locations in the environment (firing fields[1]). As a rat crosses successive firing fields, the corresponding place cells are maximally activated one after the other, representing the ongoing trajectory in 'real' time, that is, at the behavioral timescale. However, given that successive firing fields overlap with each other, the respective spike trains are actually intermingled at a faster timescale. Notably, in each cycle of the ongoing theta rhythm (~8 Hz), individual place cell bursts also tend to occur in the same order representing the past, present and future locations of the rat[2–6]. These theta sequences again reflect the ongoing trajectory, but at a highly accelerated (5–10×) speed. This would be conducive for plasticity processes possibly underlying the formation of initial episodic-like memory traces[7,8]. The same sequences are later replayed during subsequent rest and sleep supporting memory consolidation[9–12].

At the single-cell level, as the rat moves through the firing field of a place cell, the cell fires earlier and earlier in successive theta cycles, a phenomenon known as phase precession[4,13–16]. However, the mechanisms underlying the precise timing of hippocampal cell assemblies are largely unknown[13,16–26], and the functional relevance of phase precession remains debated. Although phase precession could contribute to the formation of theta sequences[2,27], additional coordination between cell assemblies is required[3–6]. Alternatively, phase precession has also been proposed to provide a temporal code for the spatial position of the rat[13,28]. We recorded hippocampal place cells and entorhinal head-direction cells during backward travel to determine individual cell properties as well as theta sequence dynamics in response to this atypical displacement. If spike timing relative to theta is under tight control from external signals involved in coding position in an allocentric reference frame, then the relation between spike theta phase and position should be maintained during backward travel. Conversely, spike theta phase could continue to represent distance traveled through the field, and, in addition, theta sequences could occur in reverse order to predict the ongoing trajectory.

RESULTS

Hippocampal place cell activity

Rats were trained to run on a miniature treadmill mounted on a model train while the train transported them in either a forward or backward direction on a 6-m-long elliptical track (**Fig. 1a**, **Supplementary Fig. 1** and **Supplementary Movie 1**). This procedure permitted continuous recordings of stable behavioral and neurophysiological data over extended periods (~10 consecutive laps) of backward travel through space. The rat's active locomotion on the treadmill was sufficient to induce strong and regular theta activity[29]. Theta frequency was similar between forward and backward travel and was slightly slower than during free running (forward travel = 7.23 ± 0.03 Hz, backward travel = 7.34 ± 0.03 Hz, free running = 7.67 ± 0.04 Hz; **Fig. 1b**,**c** and **Supplementary Fig. 2**). Theta power remained unchanged whether the rat was transported forward or backward or ran freely (forward travel = 7.57 ± 0.14, backward travel = 7.51 ± 0.13, free running = 7.84 ± 0.27, arbitrary units; **Fig. 1b**,**c** and **Supplementary Fig. 2**). Place-selective activity was also maintained across behavioral conditions. Individual place cells discharged at specific locations along the track in the three conditions (**Fig. 1d**) and were evenly distributed over the entire track (**Supplementary Fig. 3**). Firing rates and field sizes did not change with the direction of travel, although place cells tended to fire at slightly lower rates and over longer distances in the train than during free running (peak firing rates: forward travel = 8.8 ± 0.3 Hz, backward travel = 7.8 ± 0.3 Hz, free running = 9.1 ± 0.3 Hz; mean firing rates: forward travel = 5.3 ± 0.2 Hz, backward travel = 5.1 ± 0.2 Hz, free running = 5.6 ± 0.2 Hz; field sizes: forward travel = 1.73 ± 0.04 m, backward travel = 1.82 ± 0.05 m, free running = 1.22 ± 0.04 m; **Fig. 1e** and **Supplementary Fig. 3**).

To assess firing field stability during forward versus backward travel, we determined the distribution of field shifts for cells that discharged in both conditions (**Fig. 1f**) and computed the mean unsigned proportional shift σ (Online Methods). This statistic measures field shift as a

[1]Collège de France, Center for Interdisciplinary Research in Biology, Paris, France. [2]CNRS, UMR 7241, Paris, France. Correspondence should be addressed to M.Z. (michael.zugaro@college-de-france.fr).

Received 14 October 2013; accepted 13 March 2014; published online 25 March 2014; doi:10.1038/nn.3698

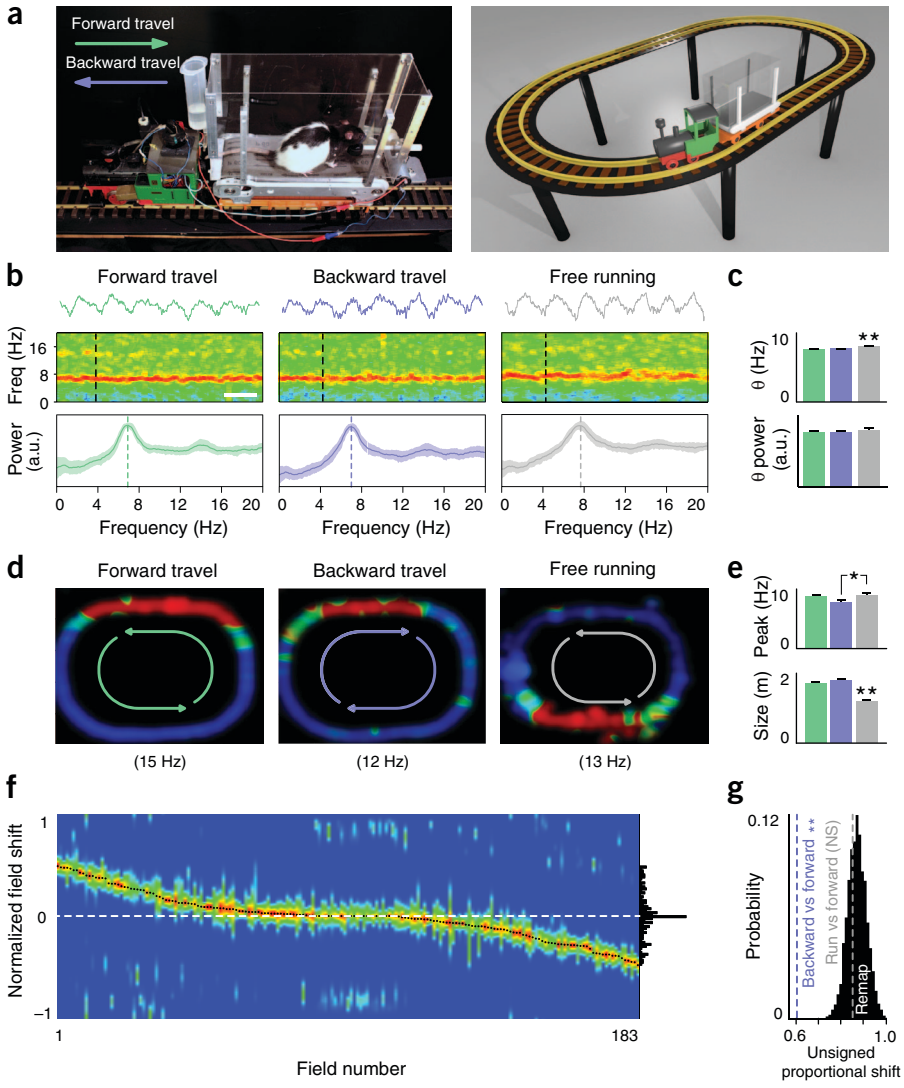

Figure 1 Theta and place selective activity are maintained during backward travel. (**a**) Rats were trained to run on a miniature treadmill (left) transported by a model train on an elliptical track (right). Forward versus backward travel (green and blue arrows, respectively) refers to the direction of displacement of the rat in space (**Supplementary Fig. 1**). (**b**) Theta oscillations were strong during forward (left) and backward (center) travel, comparable with free running (right) on the covered track. Top, local field potentials (LFPs, duration = 1 s). Center, power spectrograms (blue = minimum, red = maximum, black dashed line = time of LFP traces shown above, white calibration bar = 20 s). Bottom, power spectra (curve = mean, shaded area = s.e.m.). (**c**) Theta frequency and power during forward (green) and backward (blue) travel and during free running (gray). Data are presented as median ± standard error of the median (Kruskal-Wallis tests, $n = 164$ sessions in 5 rats, Bonferroni-corrected *post hoc* Wilcoxon rank sum tests at $P < 0.017$). Theta frequency was slightly slower on the train compared with free running ($F_{2,161} = 57.66$, $^{**}P < 0.001$), whereas theta power remained unchanged ($H_{2,161} = 2.96$, $P = 0.23$). (**d**) Firing maps of a place cell in the three behavioral conditions (arrows indicate the direction of travel). Blue indicates no firing and red indicates maximum firing (value indicated below the map). (**e**) Peak firing rates tended to decrease and field sizes tended to increase on the treadmill compared with free running. Data are presented as median ± standard error of the median (Kruskal-Wallis tests, $n = 1{,}062$ fields; peak firing rates: $H_{2,1059} = 8.08$, $^{*}P = 0.0176$; field sizes: $H_{2,1059} = 116.75$, $^{**}P < 0.001$; Bonferroni-corrected *post hoc* Wilcoxon rank sum tests at $P < 0.017$). (**f**) Spatial cross-correlograms of firing fields ($n = 183$ cells) between forward and backward travel. Black dots represent correlogram modes. Right, mode distribution. Blue indicates minimal correlation and red indicates maximal correlation. (**g**) Mean unsigned proportional shift σ between backward travel (blue dashed line) or free running (gray dashed line) and forward travel. The black area represents the distribution of σ for $n = 2{,}000$ bootstrap random remapping data sets (Online Methods and **Supplementary Fig. 4**). Place fields did not undergo random remapping between forward and backward travel ($^{**}P < 0.001$). They did remap between forward travel and free running ($P = 0.34$; not significant, NS).

proportion of field size (30 cm is a substantial shift for a 30-cm-long field, but not for a 1.5-m-long field; **Fig. 1d** and **Supplementary Fig. 4**), irrespective of shift direction (shifts in one direction should not compensate for shifts in the opposite direction). The observed value of σ was significantly lower than expected after random remapping ($P < 0.001$; **Fig. 1g**), indicating that firing fields did not undergo random remapping between forward and backward travel. In contrast, they did remap between forward travel and free running (**Fig. 1g**).

Phase precession during forward versus backward travel

Hippocampal cell assembly discharges are distributed among different phases of the ongoing theta oscillation, depending on where their place fields are located in the current trajectory. At the single-cell level, the theta phase of spikes is known to decrease linearly in successive theta cycles as the animal traverses the firing field (phase precession[13]). To compare phase precession plots during forward versus backward travel, we measured position in all analyses using a constant allocentric reference frame, independent of travel direction. Analysis of the relation between spike theta phase and location on the track (**Fig. 2a**) revealed that regression lines had opposite slopes between forward and backward travel, both within and across experiments (forward travel, −134 ± 11° m^{-1}, $n = 281$ fields; backward travel, 120 ± 9° m^{-1}, $n = 212$ fields; **Fig. 2b–d**). Notably, this was independent of locomotor commands, as it could also be observed on a subset of sessions when the rats were transported passively without treadmill walking ($n = 29$ cells in 5 rats; **Supplementary Fig. 5**). From a functional point of view, this corresponds to a degradation of the proposed hippocampal temporal code for position in allocentric space[13], as a given phase no longer coded for the same location. Instead, theta phase reflected distance traveled through the firing field, that is, position relative to the ongoing trajectory, as reported in open environments[2,30,31].

In addition, this is also pertinent to the theoretical issue that spatial information could be conveyed using either a temporal code or a rate code. Spike timing and rate have been reported to correlate[25,26], although this remains controversial[28]. We measured correlations during forward and backward travel; in both cases, as firing rate increased, phase decreased and phase variability increased (**Fig. 2e**). The apparent discrepancies among previous results[25,26,28] can be resolved by taking both position and rate into account (**Fig. 2f**).

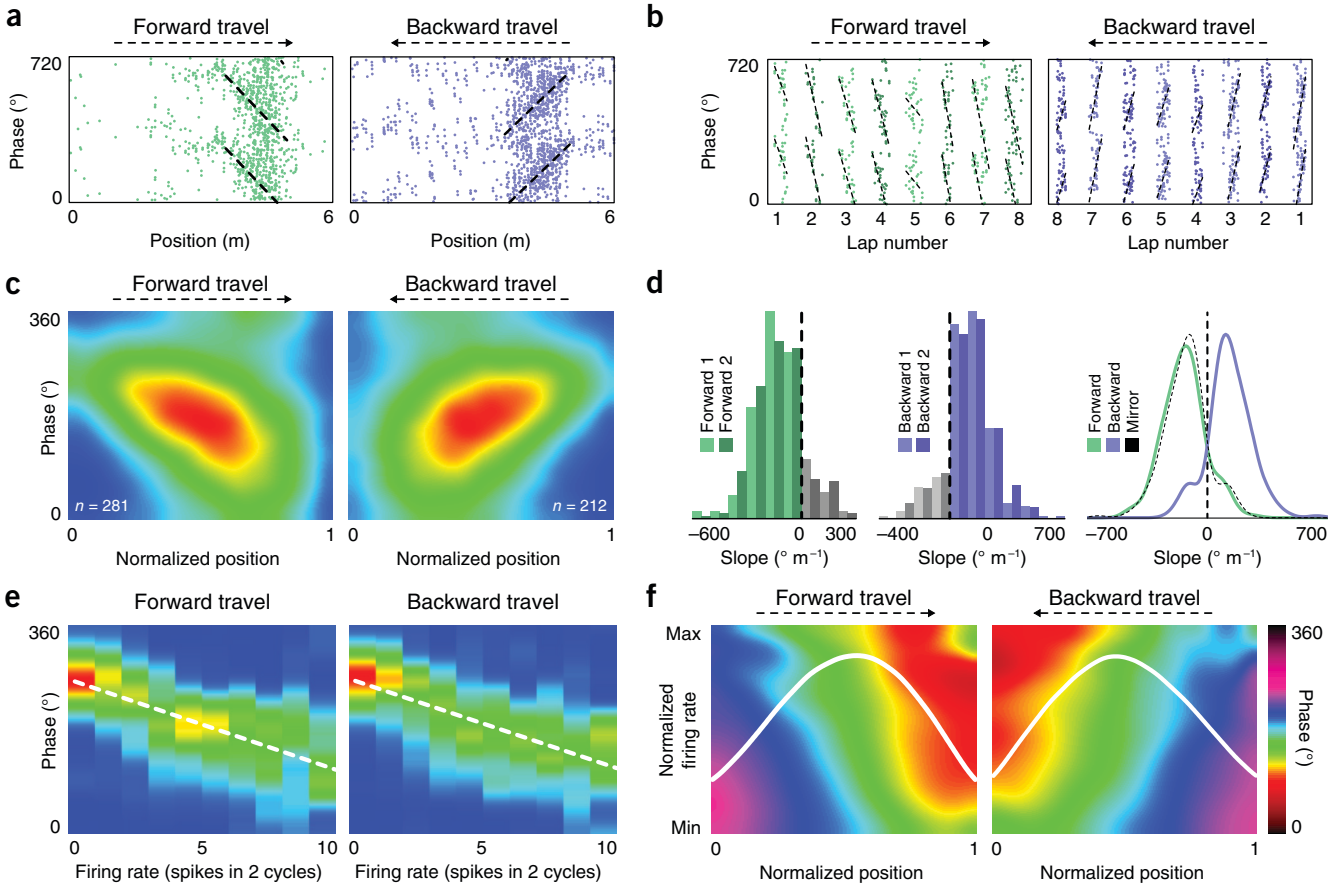

Figure 2 Hippocampal cell assemblies switched theta phases during backward travel. (**a**) An example of phase precession slope change during backward travel (measured in an allocentric reference frame). Each dot indicates the theta phase of a spike as a function of the position of the rat. Black dashed lines represent linear-circular regression lines. (**b**) Phase precession slopes remained stable across the first eight laps in each direction (same cell as in **a**). (**c**) Average normalized phase precession density plots for all place fields ($n = 281$ fields and 212 fields for forward and backward travel, respectively; blue indicates minimum, red indicates maximum). (**d**) Distribution of phase precession slopes. Slopes were stable during both forward and backward travel (left and center; forward 1, first series of laps in the forward direction; forward 2, second series; see Online Methods and **Fig. 4f**) and had opposite signs (right; compare green and dashed black curves, Kolmogorov-Smirnov, forward travel: $-134 \pm 11°\ m^{-1}$, $n = 281$ fields; backward travel: $120 \pm 9°\ m^{-1}$, $n = 212$ fields, $KS_{281,212} = 0.08$, $P = 0.389$). (**e**) Theta phase decreased with firing rate. Color heat represents the probability that spikes occur at a certain theta phase given the instantaneous firing rate. The white dashed line represents the linear-circular regression line (circular regression slopes: forward travel, –15.6° per spike per cycle, $n = 1{,}056$ cells × bins; backward travel, –15.4° per spike per cycle, $n = 1{,}036$ cells × bins; $P < 0.001$). (**f**) Spike theta phase depends on both position and firing rate. Color-coded average phase as a function of normalized position and firing rate (across all place cells). The white curve represents the firing rate as a function of position, averaged over all place fields ($n = 281$ and 212 fields for forward and backward travel, respectively). On average, phase gradually changes as indicated by following the white curve in the direction of travel. If phase depended solely on position, the plot would consist of vertical color stripes (for a given position, the phase would be constant and would not vary with rate). Conversely, if phase depended solely on rate, the plot would consist of horizontal color stripes. Instead, the diagonal bands observed here show that the phases at which spikes occur result from an inextricable combination of both position and rate.

Theta sequences during forward versus backward travel

To examine how the observed temporal reorganization of cell assemblies affects theta sequences, we decoded the trajectories represented by theta sequences (sweeps) during both forward and backward travel. To this end, we first estimated the instantaneous position of the rat on the basis of hippocampal population activity: individual firing maps were determined using the first half of the data, and the remaining data were used to reconstruct instantaneous position via Bayesian decoding of ensemble activity (**Supplementary Fig. 6** and Online Methods). We then concatenated successive positions, represented during successive fractions of ongoing theta cycles, to yield individual sweeps (**Fig. 3a**). Finally, sweeps were averaged over time (**Supplementary Fig. 7**) and sessions (**Fig. 3b**), yielding an overall estimate of the trajectories represented by theta sequences. Consistent with the direction of travel, during forward travel, the sweeps started behind the actual position of the rat and ended in front of it, and during backward travel, the sweeps started in front of the rat and ended behind it (**Fig. 3c**). Thus, theta sequences always successively represented past, present and future locations in each theta cycle[2,3,30,31]. Notably, this is not a simple consequence of the maintenance of phase precession in individual neurons, as phase precession alone cannot fully account for theta sequences, which require additional precise coordination between participating assemblies[3,4,6].

Entorhinal head-direction cell activity

Entorhinal head-direction cells selectively discharge when the head of the animal is oriented in a specific direction, generally consistent with travel direction[32]. In theory, they could therefore contribute to temporally organizing hippocampal cell assemblies so that they reflect ongoing trajectories. Contrary to this view, however, we found that the

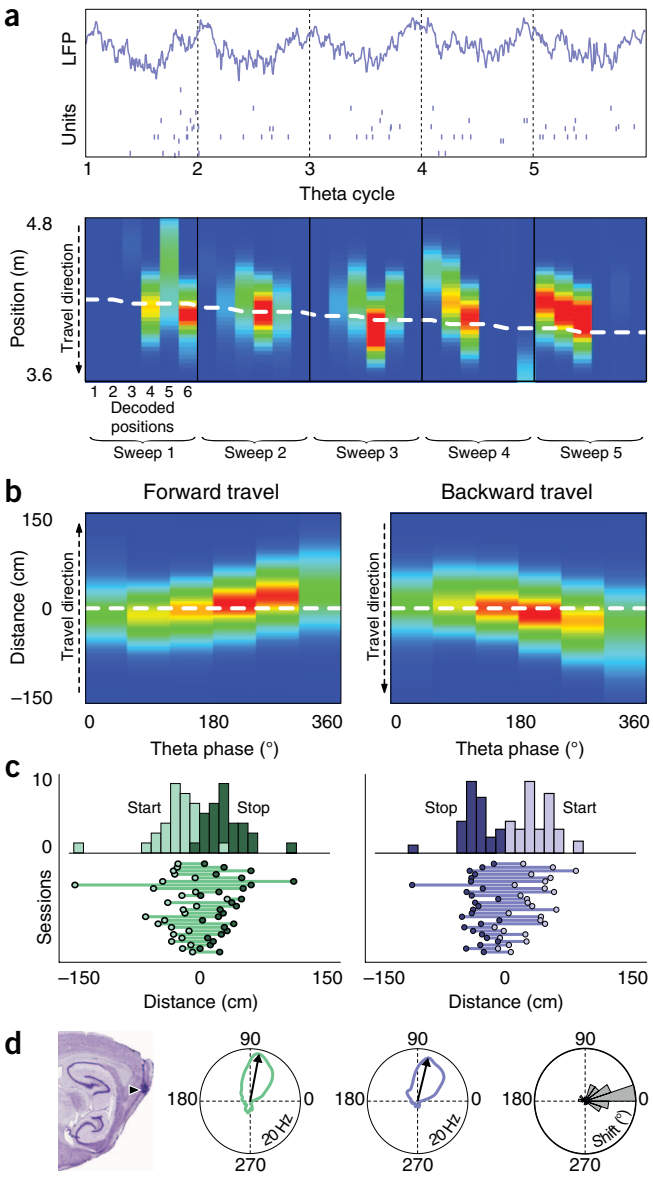

Figure 3 Theta sequences reverse to correctly predict ongoing trajectory during backward travel. (**a**) Top, LFP and spikes (vertical ticks) emitted by 34 simultaneously recorded place cells during five examples of consecutive theta cycles (dashed lines) of backward travel. Bottom, Bayesian reconstruction of the position of the rat (blue indicates minimum probability, red indicates maximum probability) based on spiking activity during successive subcycles of the theta oscillation. The dashed white line represents the actual position of the rat. (**b**) Average ($n = 26$ sessions in 4 rats) Bayesian reconstruction of the position estimated across individual theta subcycles, relative to the actual position (dashed white line). (**c**) Reconstructed trajectory start (hollow circles) and stop (filled circles) positions ($x < 0$ behind, $x > 0$ in front) relative to actual position ($x = 0$) in individual sessions. During forward travel, the sweeps started 26.9 ± 5.5 cm behind the actual position of the rat (t test, $n = 26$ sessions, $t_{25} = -4.90$, $P < 0.001$) and ended 27.7 ± 4.2 cm in front of it ($t_{25} = 6.54$, $P < 0.001$); during backward travel, the sweeps started 31.7 ± 3.5 cm in front of the rat ($t_{25} = 5.84$, $P < 0.001$) and ended 25.4 ± 4.3 cm behind it ($t_{25} = -9.09$, $P < 0.001$). (**d**) The preferred direction of head-direction cells recorded in medial entorhinal cortex did not change between forward (green curve, example cell) and backward (blue curve) travel (arrowhead on sagittal brain slice indicates the electrode tip). The gray circular histogram shows the distribution of preferred direction shifts (V test against 180°, $n = 56$ head direction cells in 5 rats, $V_{56} = 35.48$, $P < 0.001$).

preferred directions of head-direction cells remained stable between forward and backward travel (mean deviation angle = 19.5°, $n = 56$ head-direction cells; **Fig. 3d**). By dissociating head and travel direction, our protocol provides direct evidence that head-direction cells do signal the direction of the head in space, rather than the direction of travel through space. Thus, head direction cells cannot account for the reversed order of cell firing observed during backward travel.

DISCUSSION

Several theoretical frameworks have been proposed to account for phase precession and the precise timing of cell assemblies in each theta cycle. We tested specific predictions of these models (note that, although phase precession is most often studied in hippocampal pyramidal cells, it has also been documented in interneurons[33,34] as well as in other brain areas[14,35,36]; these could share similar mechanisms, although this remains unknown).

Detuned oscillator models posit that the membrane potential of place cells oscillates slightly faster than the theta rhythm; the progressive phase shift between these two oscillators results in phase precession[13,19,37–41]. In the simplest version of the model, the oscillators would be unaltered during backward travel and would continue to oscillate faster than the theta rhythm (prediction A; **Fig. 4a**). Consistent with this, place cell bursts recurred slightly faster than theta in both directions (forward travel = 1.024 ± 0.001 cycle^{-1}; backward travel = 1.022 ± 0.001 cycle^{-1}; **Fig. 4a** and Online Methods). However, we have previously provided evidence that resetting the hippocampal oscillators does not affect phase precession, a finding that was difficult to reconcile with this first version of the model[17]. In the two-dimensional version of the model, phase precession is instead inherited from entorhinal grid cells and requires multiple neuronal oscillators[19]. An important feature of this model is that the direction of travel is signaled by head-direction cells. To account for phase precession during backward travel (**Fig. 2**), their preferred directions should therefore shift by 180°; otherwise the neuronal oscillators would become slower than theta and place fields would increase in size (prediction B; **Fig. 4a**). This is not consistent with our data (**Figs. 1e** and **3d**), indicating that information about travel direction must be provided by different, as of yet undetermined, cell types.

A related model[18] was based on a similar principle, but with different underlying mechanisms: place cells also oscillate more rapidly than theta, but theta does not interfere with membrane oscillations; instead, theta is the mere combined, large-scale sum of time-shifted cell oscillations and it oscillates more slowly than its constituents (also see ref. 42; **Fig. 4b**). Consistent with this, we confirmed that population spike bursts and theta had similar frequencies during both forward (population, 7.28 ± 0.05 Hz; theta, 7.25 ± 0.03 Hz; **Fig. 4b**) and backward (population, 7.40 ± 0.05 Hz; theta, 7.35 ± 0.03 Hz; **Fig. 4b**) travel. Furthermore, as predicted by the model, the difference between theta and single cell frequencies ($f_0 - f_\theta$; **Fig. 4b**) was inversely proportional to individual field sizes ($d\Phi/L$; **Fig. 4b** and Online Methods). However, given that the mechanism underlying time shifts between cellular oscillators has not been explicitly described, it is unclear whether theta sequences would be expected to reverse during backward travel (**Fig. 4b**), as we observed here.

A second class of models is based on network properties of the hippocampal system[20–23,43–45]. Whether phase precession results from synaptic transmission delays between asymmetrically connected CA3 cells[20–22,44,45] or spatially shifted inputs from the entorhinal cortex, dentate gyrus and/or CA3 (ref. 43), the relation between the phase of spikes relative to theta and position would not depend on travel direction

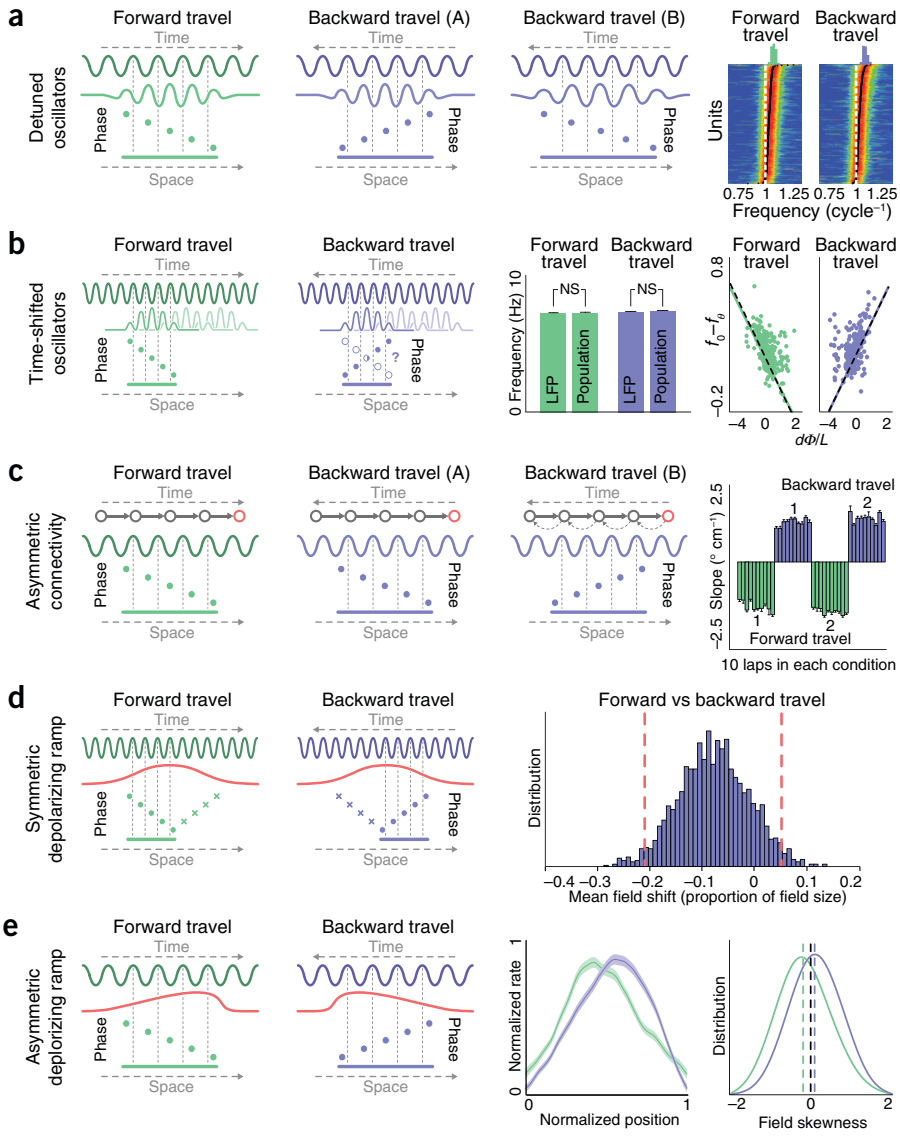

Figure 4 Tests of specific predictions of theoretical models of phase precession. (**a**–**e**) Models of phase precession, their respective theoretical predictions for the relation between spike phase and position during backward travel, and experimental tests of further specific predictions. (**a**) Units oscillate faster than theta. Power spectra of unit spike trains measured relative to theta (dashed white line indicates theta frequency). Black dots indicate spectral modes. (**b**) Left graph, population spike trains and theta oscillate at similar frequencies. Data are presented as mean ± s.e.m. (*t* test, $n = 57$ sessions in 5 rats; forward travel, $t_{56} = -0.6$, $P = 0.55$; backward travel, $t_{56} = -1.07$, $P = 0.29$). Right graph, differences between unit and LFP frequencies are inversely proportional to individual field sizes (dashed lines indicates predictions; continuous lines indicate linear regressions; regression slopes: –0.152 ± 0.010 and 0.160 ± 0.009, not significantly different from ± 1/2π, *t* test for slopes, $n = 280$ fields, $t_{278} = 0.043$, $P = 0.966$, and $n = 212$ fields, $t_{210} = 0.007$, $P = 0.995$, respectively; Online Methods). (**c**) Phase precession slopes remained stable across individual laps and did not progressively change when travel direction changed. Data are presented as median slope ± standard error of the median (Kruskal-Wallis tests; forward travel 1, $n = 1{,}212$ slopes, $H_{9,1202} = 9.32$, $P = 0.41$; backward travel 1, $n = 1{,}094$ slopes, $H_{9,1084} = 6.05$, $P = 0.73$; forward travel 2, $n = 791$ slopes, $H_{9,781} = 11.18$, $P = 0.26$; backward travel 2, $n = 598$ slopes, $H_{9,588} = 10.23$, $P = 0.33$). (**d**) Firing fields shifted on average by only ~10% of their length. Bars indicate the distribution of mean field shifts (bootstrap, $n = 2{,}000$), the plain red line represents the mean and the dashed red lines represent the 95% confidence interval. (**e**) Fields were skewed in the opposite direction during backward travel. Left graph, average firing field (curve represents mean, shaded area represents s.e.m.). Right graph, distribution of skewness values for all place fields (green and blue dashed lines represent median skewness). The median skewness was negative (–0.188 ± 0.031, $n = 329$ fields) during forward travel and became positive (0.099 ± 0.031, $n = 284$ fields) during backward travel (distribution significantly different from forward travel, Kolmogorov-Smirnov test, $KS_{329,284} = 0.249$, $P < 0.001$).

(prediction A; **Fig. 4c**); this is at odds with our results (**Fig. 2**). One possibility would be that weak reciprocal connections (prediction B; **Fig. 4c**) become dominant during backward travel, either following plastic changes induced by repeated activation of place cells in reverse order or via the gating influence of a directional signal[46]. However, single lap phase precession slopes did not change progressively across successive laps when the direction of travel was changed (**Fig. 4c**). Furthermore, the fact that head-direction cell preferred directions did not shift by 180° between forward and backward travel (**Fig. 3**) implies that they cannot provide the directional gating signal required by the model.

Yet another possibility is that phase precession results from an interaction between slowly increasing and then decreasing excitation and theta-paced inhibition as the rat traverses the place field[24–26,47,48]. To avoid generating phase-recessing spike bursts beyond the peak of excitation, these models posit either that adaptation processes prevent the neuron from firing on the descending phase of excitation[25] (**Fig. 4d**) or that asymmetric excitation abruptly returns to baseline, preventing further firing[26] (**Fig. 4e**). These models correctly predict the relation between phase and position that we observed. In the first variant of these models[25], the hypothesized adaptation mechanism predicts that, during backward travel, firing fields should systematically shift in the opposite direction by an amount equal to their own length (**Fig. 4d**). However, the average shift (–0.077 ± 0.067) that we observed was significantly different from –1 ($P < 0.01$), but not from 0 ($P > 0.05$, bootstrap confidence intervals, $n = 2{,}000$ iterations; **Fig. 4d** and Online Methods), inconsistent with the theoretical prediction. In the second variant[26], asymmetric excitation curves predict that firing fields would be skewed in the direction of travel[49]. Consistent with this, the median skewness was negative (–0.188 ± 0.031, $n = 329$ fields) during forward travel and became positive (0.099 ± 0.031, $n = 284$ fields) during backward travel (**Fig. 4e**).

In summary, we found that the order in which place cells were activated in theta sequences is reversed during backward travel. Thus, theta sequences continued to predict the ongoing trajectory despite the atypical displacement. At the single-cell level, phase precession coded for distance traveled through the firing field, and this occurred independently

of actual locomotor movements. Finally, head-direction cells maintained their preferred firing directions during backward travel, indicating that these cells do not signal travel direction, as has been assumed by several computational models. Thus, our results should inspire further development of both current and new computational models of hippocampal theta phase precession and theta sequences.

METHODS

Methods and any associated references are available in the online version of the paper.

Note: Any Supplementary Information and Source Data files are available in the online version of the paper.

ACKNOWLEDGMENTS

We thank S. Doutremer, M.-A. Thomas, Y. Dupraz and S. Rateau for technical support, M. Bechecat, L. Safra, C. Lopes Dias, H. Gao and N. Maingret for assistance with experiments, F. Sargolini and P.-Y. Jacob for advice on entorhinal recordings, and S.I. Wiener, S. Sara, K. Benchenane and N. Maingret for comments on the manuscript. This work was supported by the International Human Frontiers Science Program Organization (CDA0061/2007-C), the Région Île-de-France (A.C.), the Collège de France (A.C.) and the Fondation pour la Recherche Médicale (G.G.).

AUTHOR CONTRIBUTIONS

A.C. and M.Z. designed the study. A.C. and G.G. performed the hippocampal recordings and data processing. A.C. and C.D. performed the entorhinal recordings and data processing. A.C., K.E.K. and M.Z. analyzed the data. A.C. and M.Z. wrote the manuscript.

COMPETING FINANCIAL INTERESTS

The authors declare no competing financial interests.

1. O'Keefe, J. & Nadel, L. *The Hippocampus as a Cognitive Map* (Calendron Press, Oxford, 1978).
2. Skaggs, W.E., Mcnaughton, B.L., Wilson, M.A. & Barnes, C.A. Theta phase precession in hippocampal neuronal populations and the compression of temporal sequences. *Hippocampus* **6**, 149–172 (1996).
3. Dragoi, G. & Buzsáki, G. Temporal encoding of place sequences by hippocampal cell assemblies. *Neuron* **50**, 145–157 (2006).
4. Maurer, A.P., Cowen, S.L., Burke, S.N. & Barnes, C.A. & McNaughton, B.L. Organization of hippocampal cell assemblies based on theta phase precession. *Hippocampus* **16**, 785–794 (2006).
5. Foster, D.J. & Wilson, M.A. Hippocampal theta sequences. *Hippocampus* **17**, 1093–1099 (2007).
6. Itskov, V., Pastalkova, E., Mizuseki, K., Buzsaki, G. & Harris, K.D. Theta-mediated dynamics of spatial information in hippocampus. *J. Neurosci.* **28**, 5959–5964 (2008).
7. Gupta, A.S. & Van Der Meer, M.A., Touretzky, D.S. & Redish, A.D. Segmentation of spatial experience by hippocampal theta sequences. *Nat. Neurosci.* **15**, 1032–1039 (2012).
8. Robbe, D. & Buzsáki, G. Alteration of theta timescale dynamics of hippocampal place cells by a cannabinoid is associated with memory impairment. *J. Neurosci.* **29**, 12597–12605 (2009).
9. Buzsáki, G. Two-stage model of memory trace formation: a role for "noisy" brain states. *Neuroscience* **31**, 551–570 (1989).
10. Girardeau, G., Benchenane, K., Wiener, S.I., Buzsáki, G. & Zugaro, M.B. Selective suppression of hippocampal ripples impairs spatial memory. *Nat. Neurosci.* **12**, 1222–1223 (2009).
11. Ego-Stengel, V. & Wilson, M.A. Disruption of ripple-associated hippocampal activity during rest impairs spatial learning in the rat. *Hippocampus* **20**, 1–10 (2010).
12. Jadhav, S.P., Kemere, C., German, P.W. & Frank, L.M. Awake hippocampal sharp-wave ripples support spatial memory. *Science* **336**, 1454–1458 (2012).
13. O'Keefe, J. & Recce, M. Phase relationship between hippocampal place units and the EEG theta rhythm. *Hippocampus* **3**, 317–330 (1993).
14. Hafting, T., Fyhn, M., Bonnevie, T., Moser, M.-B. & Moser, E.I. Hippocampus-independent phase precession in entorhinal grid cells. *Nature* **453**, 1248–1252 (2008).
15. Dupret, D., O'Neill, J., Pleydell-Bouverie, B. & Csicsvari, J. The reorganization and reactivation of hippocampal maps predict spatial memory performance. *Nat. Neurosci.* **13**, 995–1002 (2010).
16. Harvey, C.D., Collman, F. & Dombeck, D.A. & Tank, D.W. Intracellular dynamics of hippocampal place cells during virtual navigation. *Nature* **461**, 941–946 (2009).
17. Zugaro, M.B., Monconduit, L. & Buzsáki, G. Spike phase precession persists after transient intrahippocampal perturbation. *Nat. Neurosci.* **8**, 67–71 (2005).
18. Geisler, C. *et al.* Temporal delays among place cells determine the frequency of population theta oscillations in the hippocampus. *Proc. Natl. Acad. Sci. USA* **107**, 7957–7962 (2010).
19. Burgess, N. Grid cells and theta as oscillatory interference: theory and predictions. *Hippocampus* **18**, 1157–1174 (2008).
20. Jensen, O. & Lisman, J.E. Hippocampal CA3 region predicts memory sequences: accounting for the phase precession of place cells. *Learn. Mem.* **3**, 279–287 (1996).
21. Tsodyks, M.V., Skaggs, W.E., Sejnowski, T.J. & McNaughton, B.L. Population dynamics and theta rhythm phase precession of hippocampal place cell firing: a spiking neuron model. *Hippocampus* **6**, 271–280 (1996).
22. Wallenstein, G.V. & Hasselmo, M.E. GABAergic modulation of hippocampal population activity: sequence learning, place field development, and the phase precession effect. *J. Neurophysiol.* **78**, 393–408 (1997).
23. Losonczy, A., Zemelman, B.V., Vaziri, A. & Magee, J.C. Network mechanisms of theta related neuronal activity in hippocampal CA1 pyramidal neurons. *Nat. Neurosci.* **13**, 967–972 (2010).
24. Kamondi, A., Acsády, L., Wang, X.J. & Buzsáki, G. Theta oscillations in somata and dendrites of hippocampal pyramidal cells in vivo: activity-dependent phase-precession of action potentials. *Hippocampus* **8**, 244–261 (1998).
25. Harris, K.D. *et al.* Spike train dynamics predicts theta-related phase precession in hippocampal pyramidal cells. *Nature* **417**, 738–741 (2002).
26. Mehta, M.R., Lee, A.K. & Wilson, M.A. Role of experience and oscillations in transforming a rate code into a temporal code. *Nature* **417**, 741–746 (2002).
27. Pastalkova, E., Itskov, V., Amarasingham, A. & Buzsáki, G. Internally generated cell assembly sequences in the rat hippocampus. *Science* **321**, 1322–1327 (2008).
28. Huxter, J., Burgess, N. & O'Keefe, J. Independent rate and temporal coding in hippocampal pyramidal cells. *Nature* **425**, 828–832 (2003).
29. Terrazas, A. *et al.* Self-motion and the hippocampal spatial metric. *J. Neurosci.* **25**, 8085–8096 (2005).
30. Burgess, N., Recce, M. & O'Keefe, J. A model of hippocampal function. *Neural Netw.* **7**, 1065–1081 (1994).
31. Huxter, J.R., Senior, T.J., Allen, K. & Csicsvari, J. Theta phase-specific codes for two-dimensional position, trajectory and heading in the hippocampus. *Nat. Neurosci.* **11**, 587–594 (2008).
32. Sargolini, F. *et al.* Conjunctive representation of position, direction, and velocity in entorhinal cortex. *Science* **312**, 758–762 (2006).
33. Maurer, A.P., Cowen, S.L., Burke, S.N. & Barnes, C.A. & McNaughton, B.L. Phase precession in hippocampal interneurons showing strong functional coupling to individual pyramidal cells. *J. Neurosci.* **26**, 13485–13492 (2006).
34. Ego-Stengel, V. & Wilson, M.A. Spatial selectivity and theta phase precession in CA1 interneurons. *Hippocampus* **17**, 161–174 (2007).
35. Kim, S.M., Ganguli, S. & Frank, L.M. Spatial information outflow from the hippocampal circuit: distributed spatial coding and phase precession in the subiculum. *J. Neurosci.* **32**, 11539–11558 (2012).
36. Jones, M.W. & Wilson, M.A. Phase precession of medial prefrontal cortical activity relative to the hippocampal theta rhythm. *Hippocampus* **15**, 867–873 (2005).
37. Geisler, C., Robbe, D., Zugaro, M., Sirota, A. & Buzsáki, G. Hippocampal place cell assemblies are speed-controlled oscillators. *Proc. Natl. Acad. Sci. USA* **104**, 8149–8154 (2007).
38. Booth, V. & Bose, A. Neural mechanisms for generating rate and temporal codes in model CA3 pyramidal cells. *J. Neurophysiol.* **85**, 2432–2445 (2001).
39. Yamaguchi, Y. A theory of hippocampal memory based on theta phase precession. *Biol. Cybern.* **89**, 1–9 (2003).
40. Lengyel, M., Szatmáry, Z. & Erdi, P. Dynamically detuned oscillations account for the coupled rate and temporal code of place cell firing. *Hippocampus* **13**, 700–714 (2003).
41. Sato, N. & Yamaguchi, Y. Memory encoding by theta phase precession in the hippocampal network. *Neural Comput.* **15**, 2379–2397 (2003).
42. Burgess, N., O'Keefe, J. & Recce, M. Using hippocampal place cells' for navigation, exploiting phase coding. *Adv. Neural Inf. Process. Syst.* **5**, 923–936 (1993).
43. Chance, F.S. Hippocampal phase precession from dual input components. *J. Neurosci.* **32**, 16693–16703 (2012).
44. Castro, L. & Aguiar, P. Phase precession through acceleration of local theta rhythm: a biophysical model for the interaction between place cells and local inhibitory neurons. *J. Comput. Neurosci.* **33**, 141–150 (2012).
45. Baker, J.L. & Olds, J.L. Theta phase precession emerges from a hybrid computational model of a CA3 place cell. *Cogn. Neurodyn.* **1**, 237–248 (2007).
46. Navratilova, Z., Giocomo, L.M., Fellous, J.-M., Hasselmo, M.E. & McNaughton, B.L. Phase precession and variable spatial scaling in a periodic attractor map model of medial entorhinal grid cells with realistic after-spike dynamics. *Hippocampus* **22**, 772–789 (2011).
47. Magee, J.C. Dendritic mechanisms of phase precession in hippocampal CA1 pyramidal neurons. *J. Neurophysiol.* **86**, 528–532 (2001).
48. Leung, L.S. A model of intracellular theta phase precession dependent on intrinsic subthreshold membrane currents. *J. Neurosci.* **31**, 12282–12296 (2011).
49. Mehta, M.R. & Barnes, C. & McNaughton, B.L. Experience-dependent, asymmetric expansion of hippocampal place fields. *Proc. Natl. Acad. Sci. USA* **94**, 8918–8921 (1997).

ONLINE METHODS

Animal training. Ten adult male Long-Evans rats (René Janvier), aged 3–5 months, were housed individually and maintained on a 12-h light/dark cycle. The rats were kept on a mild water restriction diet, maintained at 85% of their normal weight. Over the course of 3–4 weeks, the rats were trained to run on a miniature treadmill transported by a model train (LGB; **Fig. 1a** and **Supplementary Fig. 1**). The train moved at constant speed (~25–30 cm s^{-1}) on a 2.30-m × 1.30-m annular track. The rats received sweetened water rewards (1.25% saccharine) at two different locations on the track. During the entire training period, the rats only experienced forward travel. All experiments were in accord with institutional (CNRS Comité Opérationnel pour l'Éthique dans les Sciences de la Vie), international (US National Institutes of Health guidelines) standards and legal regulations (Certificat no. B751756, Ministère de l'Agriculture et de la Pêche) regarding the use and care of animals. Training and experiments took place during the day.

Electrode implantation and behavioral task. The rats were deeply anesthetized (xylazine, 0.1 ml intramuscular; pentobarbital, 40 mg per kg of body weight, intraperitoneal; 0.1 ml pentobarbital supplemented every hour). For hippocampal recordings (n = 5 rats), 8 or 16 independently movable tetrodes (groups of four twisted 13 μm tungsten wire, gold-plated to ~200 kΩ) were implanted above the hippocampus (–3.5 mm AP, ± 2.5 mm ML relative to bregma). For entorhinal recordings (n = 5 rats), 2–8 octrodes were implanted above the entorhinal cortex (0.7 mm anterior to the transverse sinus, ± 4.8 mm ML relative to bregma). Following recovery, the electrodes were progressively lowered until they reached the CA1 pyramidal layer or layers V-VI or II-III of the entorhinal cortex (**Fig. 3d**), where unit activity and local field potentials were recorded as the animals performed the task.

Experiments consisted of a series of alternating conditions (~10 laps each), including running on the treadmill while transported in the forward or backward direction and running on the covered track (**Supplementary Fig. 1**). Forward and backward travel were repeated twice (in alternation) to test for the stability of the responses (**Supplementary Fig. 4**). Experiments also included passive transportation in both directions, during which the treadmill was not activated (**Supplementary Fig. 5**). The order of the different conditions varied in a pseudo-random manner across days. At the end of the experiments, slight local lesions were induced at the tip of the electrode by injecting a weak current (30 μA). Then, the rats were deeply anesthetized with pentobarbital and perfused with 50 ml of cold saline (0.9%, wt/vol) followed by 400 ml of buffered fixative (10% paraformaldehyde, wt/vol). Brains were postfixed at 4 °C for a week, and then kept in 0.1 M phosphate-buffered saline. Brains were sliced into coronal sections (40 μm) and stained with Nissl to confirm the electrode placement.

Data acquisition and preprocessing. Brain signals were preamplified (unity-gain, Noted Bt) and acquired at 32552.083 Hz using a Digital Lynx system (Neuralynx). The head-stage was connected to the recording set up via two custom-made tethers (New England Wire). Two LEDs (green and red) attached to the tethers were used to track the animals. Moment-to-moment positions of the LEDs were recorded at 29.97 Hz, then resampled at 39.0625 Hz. For off-line spike sorting, the wide-band signals were converted, digitally high-pass filtered (nonlinear median-based filter[50]), and thresholded[51] using NDManager (L. Hazan and M. Zugaro, http://ndmanager.sourceforge.net)[52]. Extracted waveforms were sorted via a semi-automatic cluster cutting procedure using KlustaKwik (K.D. Harris, http://klustakwik.sourceforge.net)[53] and Klusters (L. Hazan, http://klusters.sourceforge.net)[52]. Neurophysiological and behavioral data were explored using NeuroScope (L. Hazan, http://neuroscope.sourceforge.net)[52]. LFPs were derived from wideband signals by downsampling all channels to 1,250 Hz. Analyses relating unit activity to theta oscillations used the LFP recorded by one of the tetrode wires.

Data analysis and statistics. Descriptive statistics are reported as mean ± s.e.m. when the underlying distribution is Gaussian-shaped (Lilliefors test at alpha = 0.01) or median ± standard error of the median otherwise. Multiple comparisons use the Kruskal-Wallis test. No statistical methods were used to pre-determine sample sizes, but our sample sizes are similar to those generally employed in the field. Data collection and analysis were not performed blind to the conditions of the experiments. All statistical tests were two-tailed.

Theta power and frequency. Power spectra and spectrograms were computed using multitaper estimation methods (http://chronux.org) from the detrended LFP signal. Theta power was measured as the mean power between 6 and 9 Hz, and frequency was measured as the mode located in the same range. Similar results were obtained when theta amplitude and frequency were computed from the Hilbert-transformed, filtered signal (**Supplementary Fig. 2b**).

Firing fields. All analyses examined data where the linear velocity of the rat was greater than 5 cm s^{-1}. Firing maps and linearized firing curves were computed using a kernel-based method[53]. The firing rate was estimated at each point x as

$$f(x) = \sum_t n_t \bullet w\left(\left|x - x_t\right|\right) / \sum_t dt \bullet w\left(\left|x - x_t\right|\right),$$

where, in a given time bin t, n_t is the number of action potentials emitted, x_t is the position of the rat, and dt is the time bin size. The kernel function w was a Gaussian of width 4.5 cm. Firing fields were defined as the set of contiguous bins containing the location of maximal firing rate, for which the firing rates exceeded 20% of the peak firing rate.

To test for random remapping across conditions, we first computed for each place cell the spatial cross-correlogram between its firing curves recorded for example during forward and backward travel, and took the mode of the cross-correlogram as the spatial shift between the two conditions. Because a 30-cm shift is a substantial change for a 30-cm-long field, but not for a 1.5-m-long field, the proportional shift was then measured as the ratio of the field shift and the average field size across the two conditions. In addition, to prevent forward shifts to compensate for backward shifts, we defined the unsigned proportional shift as the absolute value of the proportional field shift. Finally, the mean unsigned proportional shift σ measured the overall propensity of firing fields to remap between conditions. To test for random remapping, we compared the observed value of σ to the distribution of n = 2,000 surrogate values of σ generated by shuffling the identity of the cells across conditions to simulate a random rearrangement of the fields (**Supplementary Fig. 4**).

To determine whether the fields shifted by a systematic amount between forward and backward travel, the observed mean (signed) proportional shift was compared to theoretical values expected from computational models. Confidence intervals were computed using a non-parametric (bootstrap, n = 2,000) estimation method (**Fig. 4d**).

To compare the shape of firing fields during forward versus backward travel, asymmetry was assessed using lower (5%) firing rate thresholds as field boundaries, as high thresholds have been reported to yield underestimated measures of skewness[54].

Phase precession. For each firing field, spike theta phases were plotted against linearized positions on the track. Linear-circular regression was applied to determine phase precession slopes, and subsequent analyses were restricted to fields with slopes significantly ($P < 0.05$) different from zero[55]. Average phase precession density plots were constructed by normalizing the position in the firing field (from 0 to 1) and shifting the mean spike theta phase to 180°, then normalizing the resulting density plots by the total number of spikes, and averaging over cells.

To assess correlations between spike theta phase and firing rate, we counted the number of spikes emitted in two cycles centered on each individual spike as the instantaneous firing rate. Phase probability distributions for each rate level were then averaged over cells. Linear-circular regression yielded a measure of the association between the two variables.

The relation between phase, rate and position was determined by normalizing both position within the field and firing rate for each neuron, then computing the (circular) mean phase for all spikes associated with a given (position, rate) pair, and averaging over neurons.

Preferred directions. The two LEDs located above the head of the rat were used to define the instantaneous head direction. The tuning curve of a head direction cell was computed using the approach described above for place cell firing curves, but using head angle as the independent variable. Normalized firing curves were fitted with a Von Mises distribution and cells with a κ value lesser than 0.35 were discarded. The width of the Gaussian kernel was 6°. The preferred direction of a head direction cell was defined as the mode of its tuning curve.

doi:10.1038/nn.3698

Bayesian position reconstruction. The goal of this analysis was to estimate the position of the rat from the instantaneous firing rate of an ensemble of place cells. Each theta cycle was divided into six subcycles and, in each of the resulting time bins, we estimated the probability $P(x|n)$ that the rat was located at position x, given the instantaneous firing rate vector n. The analysis consisted of a training step, using the first half of the data recorded during a given session, and a test step, using the data recorded during the rest of the session (**Supplementary Fig. 6**). In the training step, we estimated the occupancy probability $P(x)$ as the normalized occupancy curve and the average firing probability $\lambda_i(x)$ at position x for each unit i as the normalized firing curve. In the test step, we first estimated in each successive theta subcycle the probability $P(n|x) = \Pi P(n_i|x)$ of the observed spike count vector for each possible position x.

This was derived from the Poisson model

$$P\left(n_i\middle|x\right) = \frac{1}{n_i!}\left(\lambda_i(x)\bullet dt\right)^{n_i} * \exp\left(-\lambda_i(x)\bullet dt\right),$$

where dt is the (variable) duration of the current theta subcycle.

We then derived the probability

$$P\left(x\middle|n\right) = P\left(n\middle|x\right)^* \; P(x) \,/\, P(n)$$

that the rat was located at position x (**Fig. 3a**). To determine where the reconstructed position was situated relative to the real position x_0 of the rat, the elements of the probability vector $P(x|n)$ were shifted circularly until the vector was centered on the bin corresponding to x_0. Finally, reconstructions from individual theta subcycles were averaged over successive cycles yielding an overall estimate of theta-scale sequences (sweeps). Sweep start and stop distances were determined via linear-circular regression.

Theta burst frequency. To compute spike phase spectra, we first converted spike times into unwrapped theta phases, then divided these by 2π, resulting in spike times expressed in units of theta cycles. Spectrograms computed from these spike trains measured frequencies relative to theta, compensating for moment-to-moment variations in theta frequency over the course of a given experiment.

50. Fiore, L., Corsini, G. & Geppetti, L. Application of non-linear filters based on the median filter to experimental and simulated multiunit neural recordings. *J. Neurosci. Methods* **70**, 177–184 (1996).
51. Quiroga, R.Q., Nadasdy, Z. & Ben-Shaul, Y. Unsupervised spike detection and sorting with wavelets and superparamagnetic clustering. *Neural Comput.* **16**, 1661–1687 (2004).
52. Hazan, L., Zugaro, M. & Buzsáki, G. Klusters, NeuroScope, NDManager: a free software suite for neurophysiological data processing and visualization. *J. Neurosci. Methods* **155**, 207–216 (2006).
53. Harris, K.D., Hirase, H., Leinekugel, X. & Henze, D.A. & Buzsáki, G. Temporal interaction between single spikes and complex spike bursts in hippocampal pyramidal cells. *Neuron* **32**, 141–149 (2001).
54. Mehta, M.R., Quirk, M.C. & Wilson, M.A. Experience-dependent asymmetric shape of hippocampal receptive fields. *Neuron* **25**, 707–715 (2000).
55. Kempter, R., Leibold, C., Buzsáki, G., Diba, K. & Schmidt, R. Quantifying circular-linear associations: Hippocampal phase precession. *J. Neurosci. Methods* **207**, 113–124 (2012).

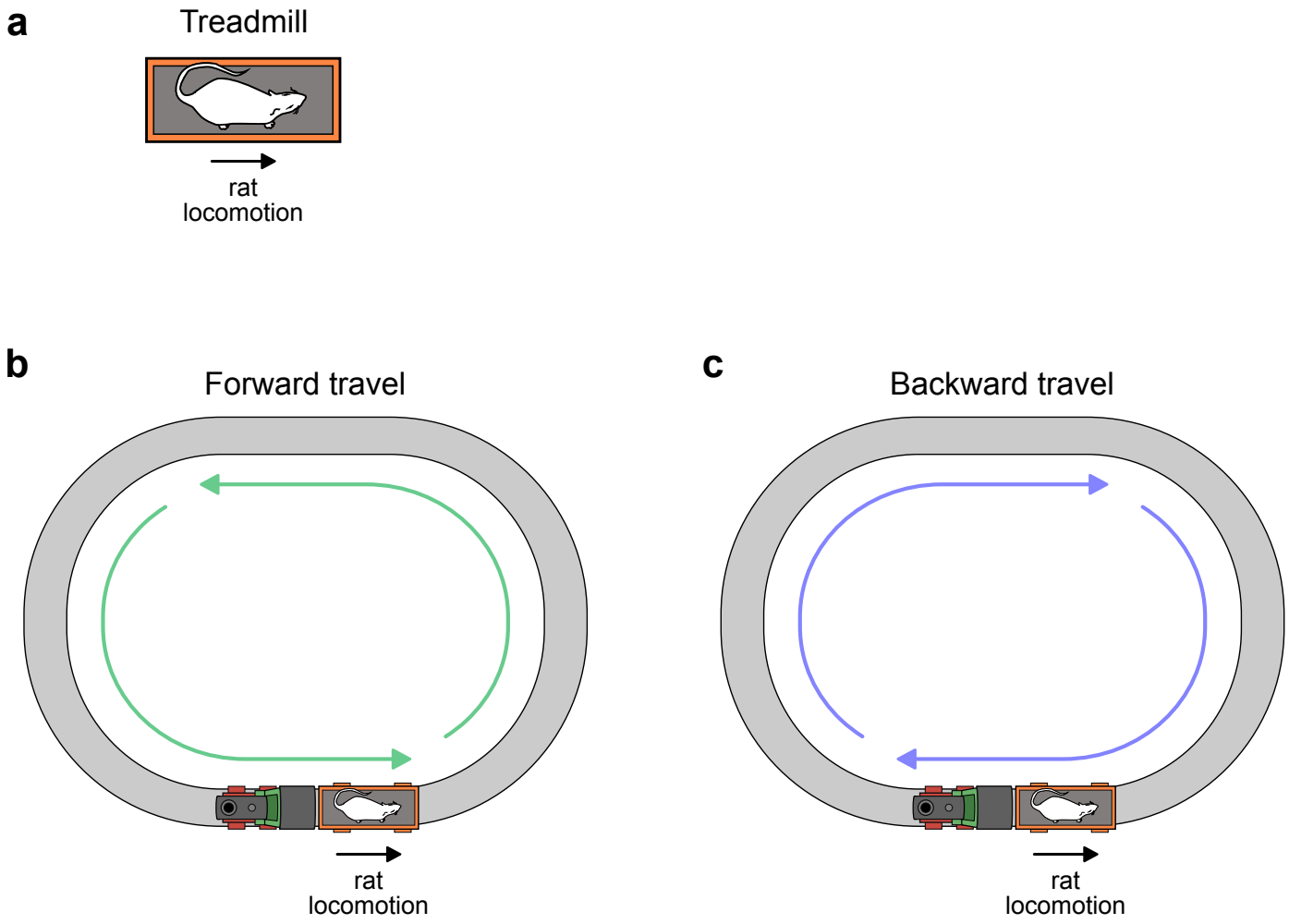

Supplementary Figure 1 Behavioral task. (**a**) Each rat was first trained to run on a miniature treadmill. The locomotor movements of the rat (black arrow) remained unchanged (speed, direction) in all subsequent behavioral conditions involving the running treadmill. (**b**) The treadmill was mounted on a model train that transported the rat on an elliptical track. Throughout this study the direction of displacement in space is considered in reference to the rat (not to the locomotive, which was located behind the rat to avoid blocking the view). Forward travel (green arrows, control) mimicked free running: the direction of travel was consistent with the locomotor movements of the rat. (**c**) During backward travel (blue arrows, test), the rat was transported backward in space, conflicting with its locomotor movements. Spurious effects of this conflict were ruled out in a subset of sessions where the treadmill was turned off (**Supplementary Fig. 5**).

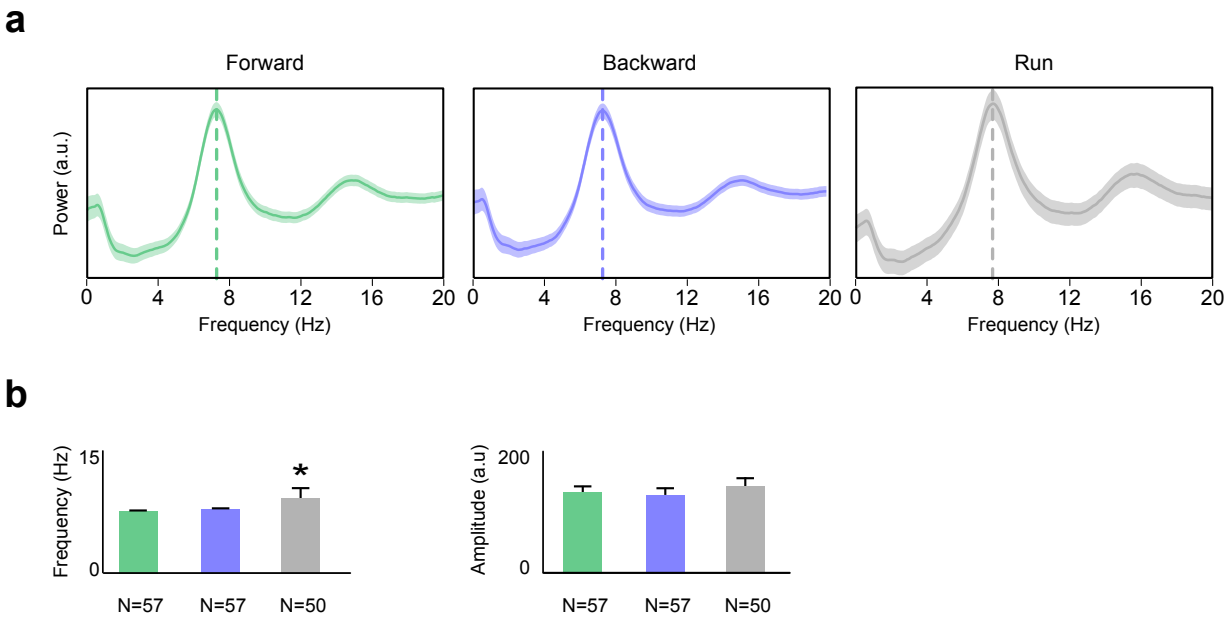

Supplementary Figure 2 Theta amplitude and frequency do not change during backward travel. (**a)** Power spectra averaged over all experiments during forward and backward travel, as well as during free run. (**b)** Mean theta frequency and amplitude computed from the band-pass filtered, Hilbert-transformed LFP signal. Frequency: forward travel, 7.4±0.1 Hz; backward travel, 7.6±0.1 Hz; free running, 7.9±1.3 Hz; amplitude (a.u.): forward travel, 132±10; backward travel, 128±10; free running, 142±15; * p<0.05).

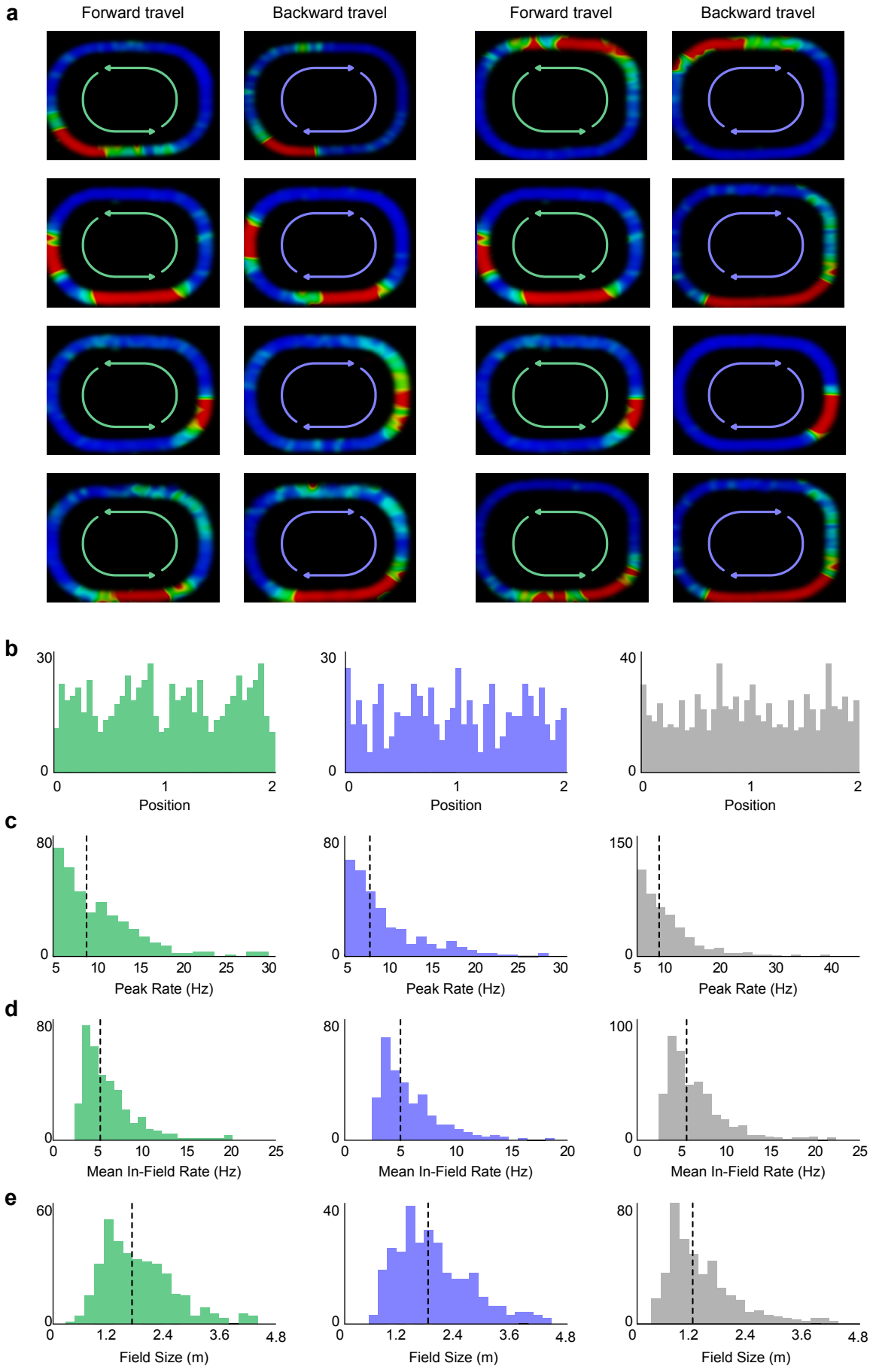

Supplementary Figure 3 Place selective activity is maintained during backward travel. (**a)** Example firing fields in each condition. (**b)** Firing field modes are evenly distributed around the circular track (Rayleigh tests, NS; forward travel in green, *n*=353 fields, backward travel in blue *n*=295 fields; free running in grey *n*=414 fields). For display purposes, the distributions are represented twice along the x axis. (**c–e)** Distributions of peak firing rates (**c**), mean in-field firing rate (**d**) and field size (**e**) during forward and backward travel, and during free running. Dashed lines: median values. Forward travel in green, *n*=353 fields, backward travel in blue *n*=295 fields; free running in grey *n*=414 fields.

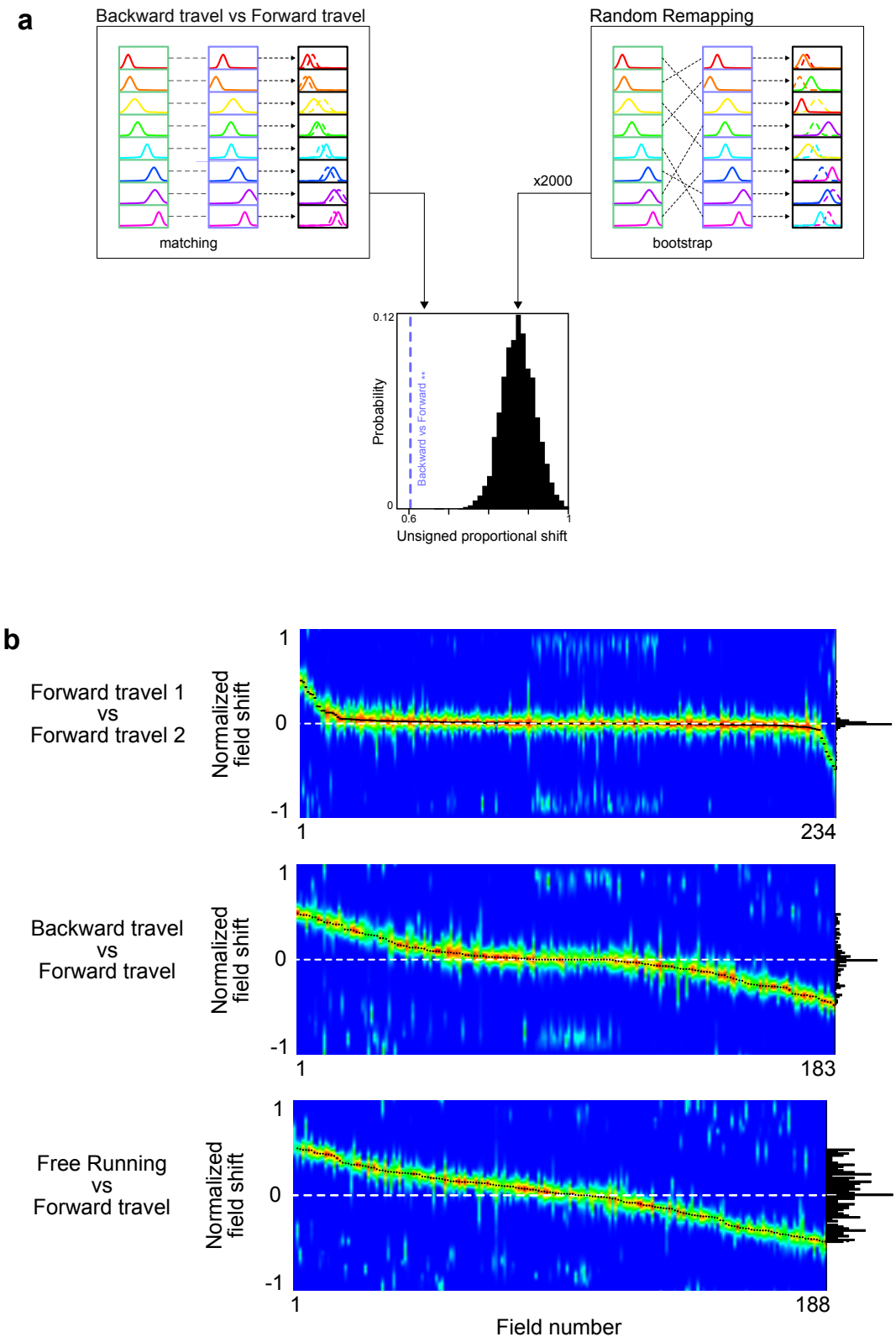

Supplementary Figure 4 Firing fields do not undergo random remapping during backward travel. (**a**) Proportional field shifts were measured between forward (green boxes) and backward (blue boxes) travel. Individual firing curve pairs (color curves) were spatially cross-correlated, the location of the mode (black dots) was expressed relative to the average field size. The mean unsigned proportional shift was then compared to the distribution obtained by shuffling cell identities 2000 times (schematic diagram on the right). (**b**) Spatial cross-correlograms comparing field locations during sucessive repetitions of forward travel (top), during forward vs backward travel (middle), and during forward travel and free running (bottom).

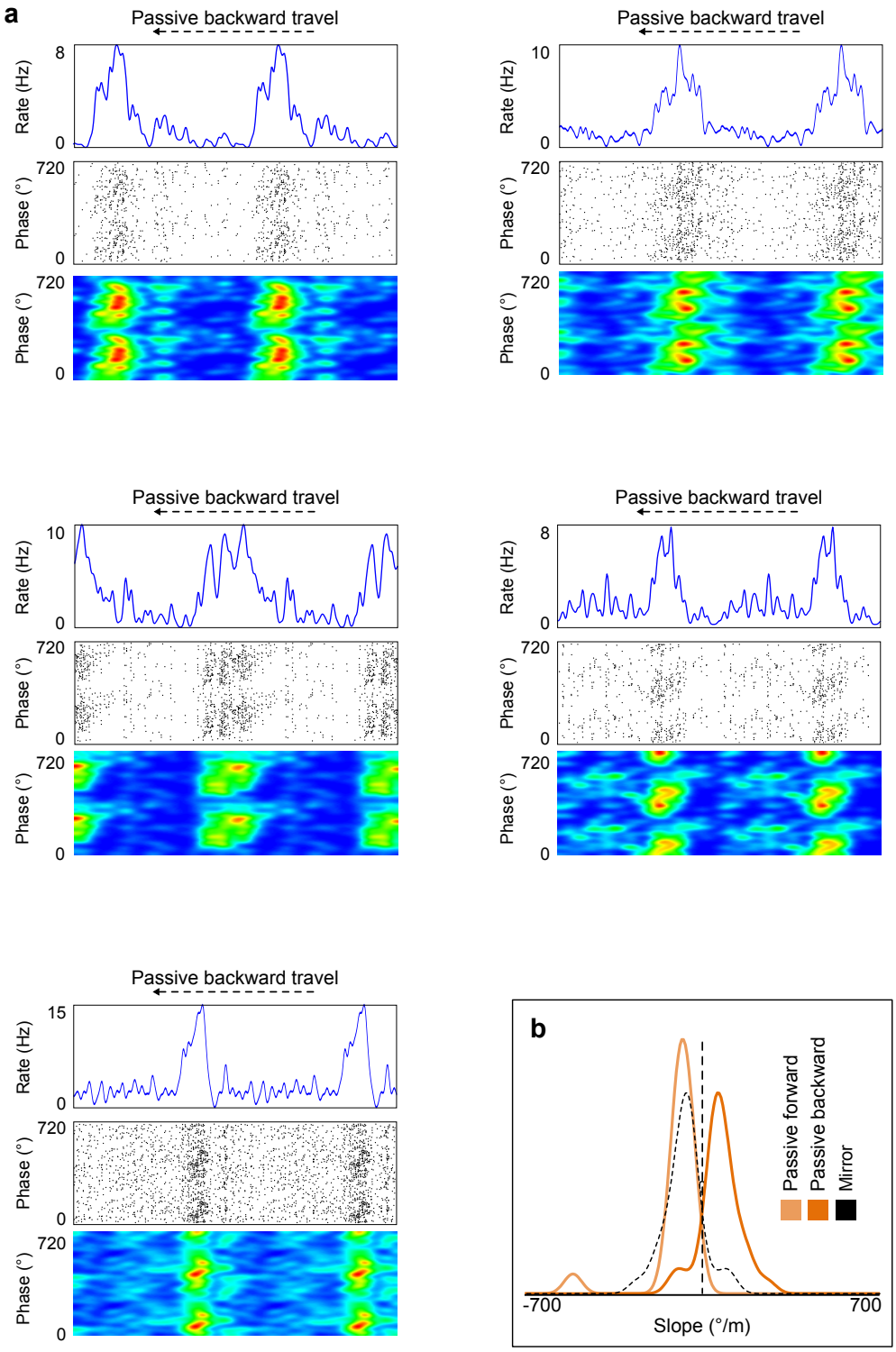

Supplementary Figure 5 Phase precession slopes reversed during passive backward travel when the treadmill was turned off. (**a**) Firing curves (blue curves), phase precession plots and density maps for five example place cells recorded during passive backward travel. (**b**) Distribution of phase precession slopes during passive forward (light orange curve, *n*=18 fields) and backward (dark orange curve, *n*=29 fields) travel. Similar to sessions where rats ran on the treadmill, slope distributions were mirror images of each other (compare light orange and dotted black curves).

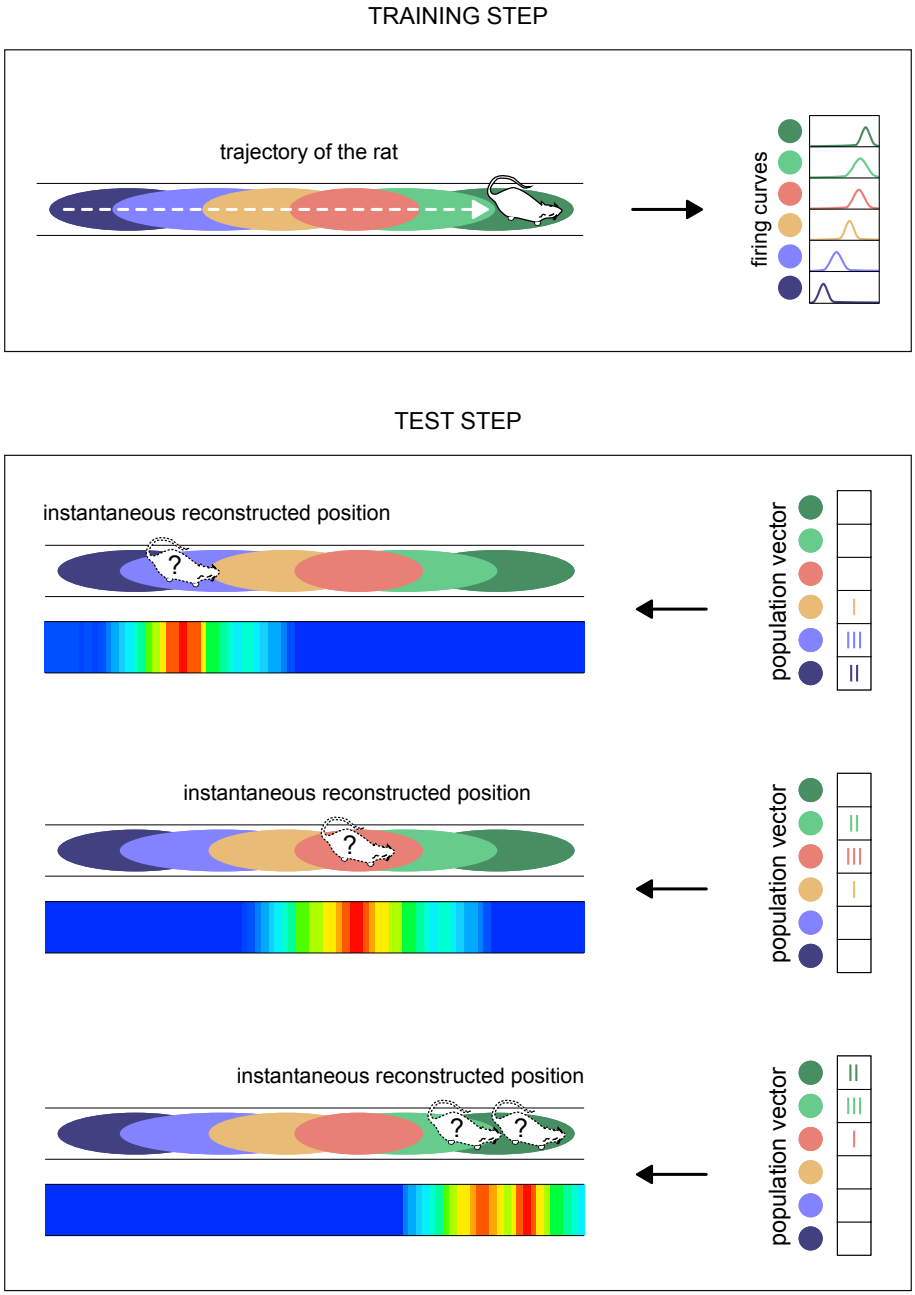

Supplementary Figure 6 Bayesian reconstruction of the instantaneous position of the rat (general principle). In the training step, the first half of the data recorded during a given session is used to determine the average firing curve of each place cell (color curves on the right; firing fields are represented as colored ellipses along the trajectory). In the test step, the instantaneous firing rates of the place cells (population vectors) are used to estimate the probability (color coded from blue to red) that the rat is located in each of the position bins on the maze. Three example reconstructions are represented. In the first and second examples, the population vector yields a high probability (in red) that the rat is located near the center of the purple (respectively, red) firing field. The third example yields a more ambiguous estimation: the probability distribution is bimodal, indicating that the rat is most probably located either near the end of the light green firing field, or near the center of the dark green firing field.

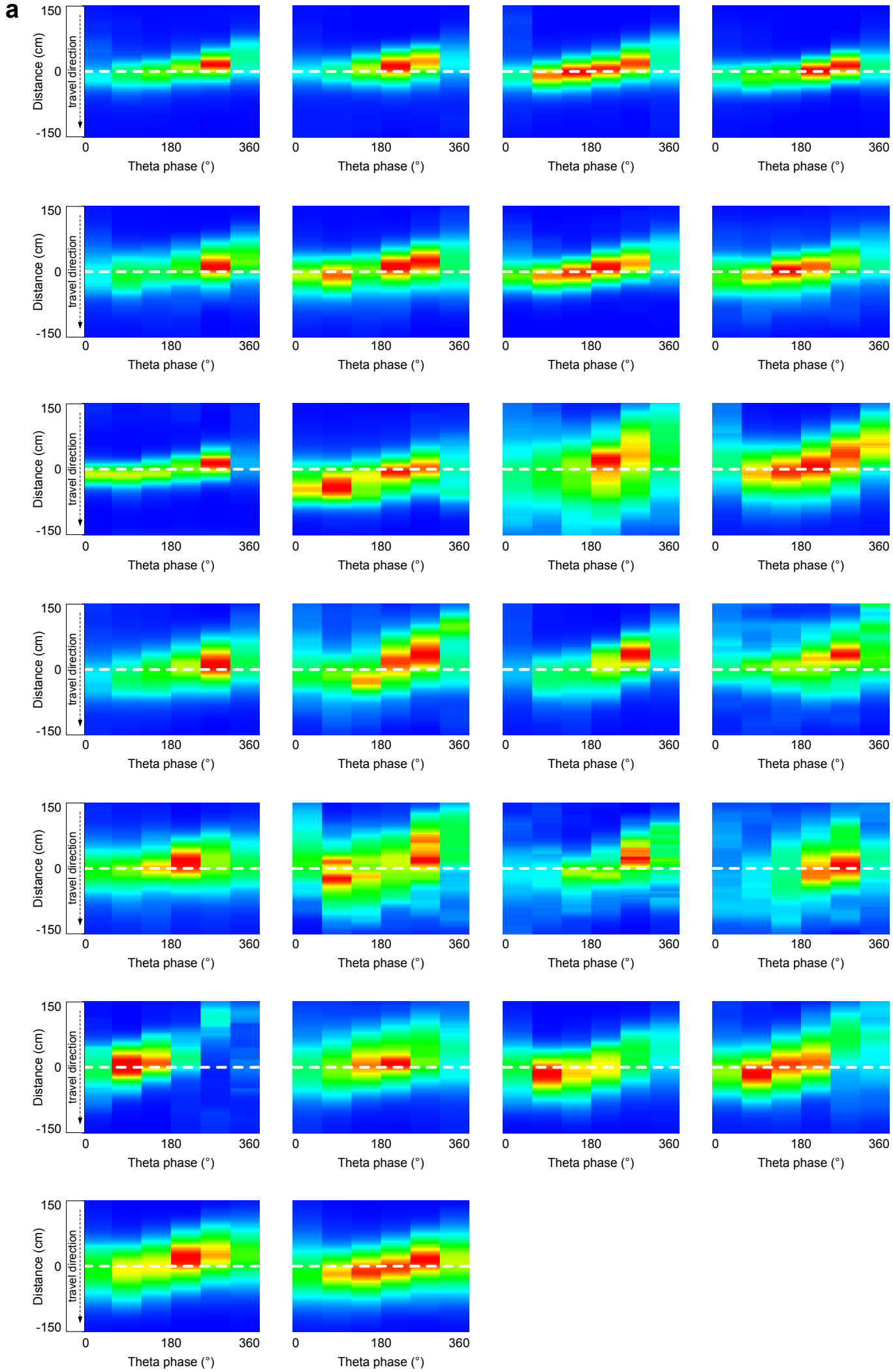

Nature Neuroscience: doi:10.1038/nn.3698

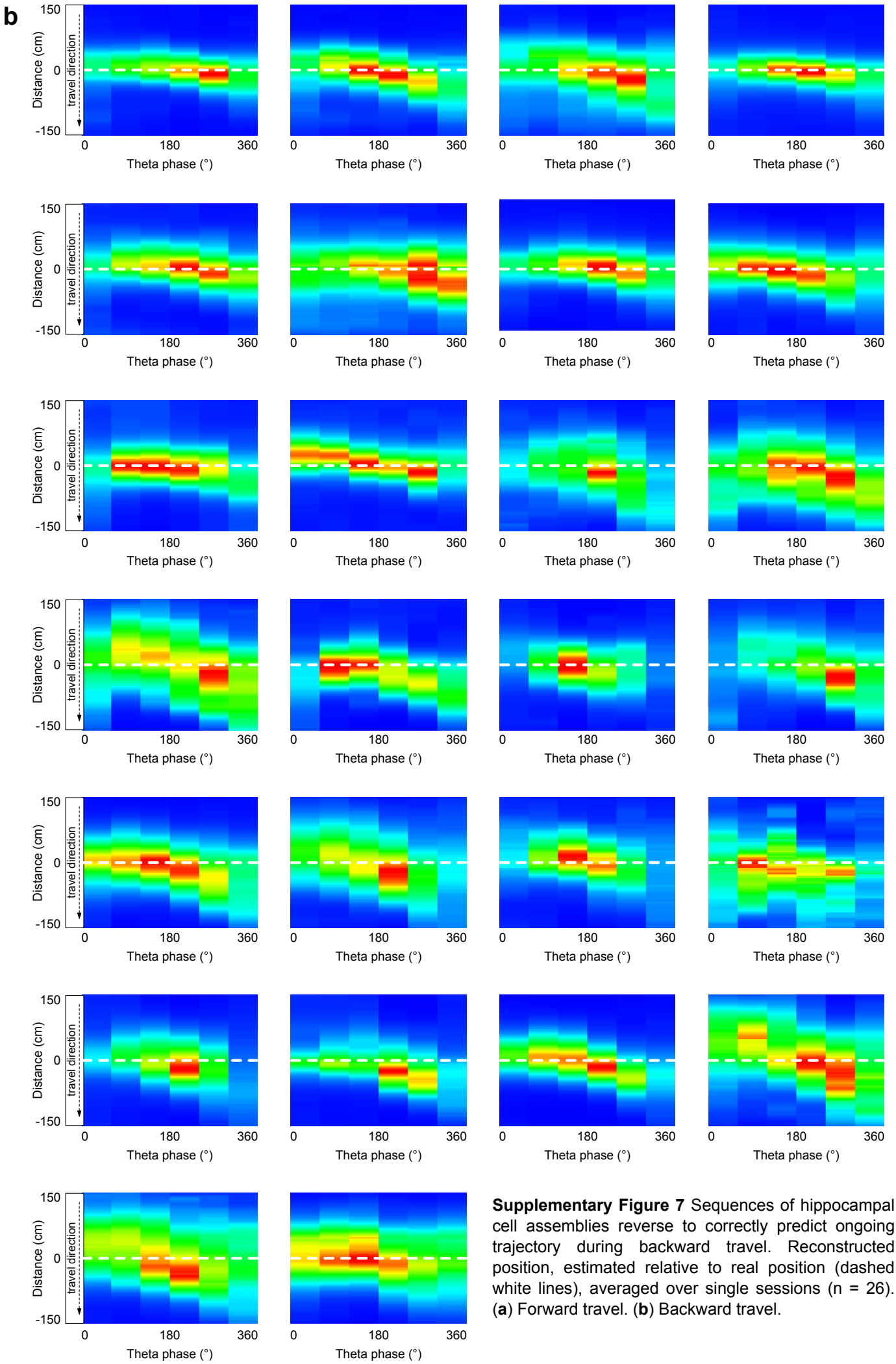

Supplementary Figure 7 Sequences of hippocampal cell assemblies reverse to correctly predict ongoing trajectory during backward travel. Reconstructed position, estimated relative to real position (dashed white lines), averaged over single sessions (n = 26). (**a**) Forward travel. (**b**) Backward travel.

Supplementary Video A rat running on the treadmill while transported backward by the train. This video file shows an implanted rat running on the treadmill during a backward travel. The rat receives sweet water reward from the black cup.